International Journal of Thermophysics, Vol. 27, No. 3, May 2006 (© 2006)
DOI: 10.1007/s10765-006-0061-2

New Transient Hot-Bridge Sensor to Measure Thermal Conductivity, Thermal Diffusivity, and Volumetric Specific Heat

U. Hammerschmidt[1,3] and V. Meier[2]

Received June 16, 2005

A high sensitivity thermoelectric sensor to measure all relevant thermal transport properties has been developed. This so-called transient hot bridge (THB) decidedly improves the state of the art for transient measurements of the thermal conductivity, thermal diffusivity, and volumetric specific heat. The new sensor is realized as a printed circuit foil of nickel between two polyimide sheets. Its layout consists of four identical strips arranged in parallel and connected for an equal-ratio Wheatstone bridge. At uniform temperature, the bridge is inherently balanced, i.e., no nulling is required prior to a run. An electric current makes the unequally spaced strips establish an inhomogeneous temperature profile that turns the bridge into an unbalanced condition. From then on, the THB produces an offset-free output signal of high sensitivity as a measure of the properties mentioned of the surrounding specimen. The signal is virtually free of thermal emf's because no external bridge resistors are needed. Each single strip is meander-shaped to give it a higher resistivity and, additionally, segmented into a long and short part to compensate for the end effect. The THB closely meets the specific requirements of industry and research institutes for an easy to handle and accurate low cost sensor. As the key component of an instrument, it allows rapid thermal-conductivity measurements on solid and fluid specimens from 0.02 to $100\,\mathrm{W\cdot m^{-1}\cdot K^{-1}}$ at temperatures up to 250°C. Measurements on some reference materials and thermal insulations are presented. These verify the preliminary estimated uncertainty of 2% in thermal conductivity.

KEY WORDS: thermal conductivity; thermal diffusivity; thermoelectric sensor; transient hot bridge; transient hot strip; volumetric specific heat.

[1] Physikalisch-Technische Bundesanstalt (PTB), Bundesallee 100, 38116 Braunschweig, Germany.
[2] Ing.-Büro Meier, Woermannstraße 33, 30455 Hannover, Germany.
[3] To whom correspondence should be addressed. E-mail: ulf.hammerschmidt@ptb.de

0195-928X/06/0500-0840/0 © 2006 Springer Science+Business Media, Inc.

1. INTRODUCTION

In 1979, Gustafsson [1] came up with a new rapid method to simultaneously measure the thermal conductivity and thermal diffusivity of solids. In his transient hot-strip (THS) technique, he first replaced the wire of the transient hot-wire (THW) method by a thin metal strip as the resistive heater and thermometer. Then, he adapted the existing THW theory to the strip equivalent to establish the appropriate THS working equation.

The basic idea behind the THS is very simple: the heat emitting surface of a strip is more than ten times larger than that of a comparable wire. Thus, (1) a strip makes better thermal contact to the surrounding solid sample and, consequently, (2) a strip liberates its heat at a smaller heat flow density. Furthermore, (3) the handling of a strip is by far not as complicated and tedious as that of a thin wire. However, despite all efforts and improvements in the method since 1979, the THS method could not win adequate recognition.

It soon turned out that, due to its larger cross-section area, the strip has the drawback of a smaller electrical resistance than a wire. Thus, the temperature-dependent voltage signal is much smaller. Therefore, often nanovoltmeters are required to measure the output signal. Moreover, most THW setups use a Wheatstone bridge configuration of two wires of different lengths (1) to minimize the offset voltage and (2) to compensate for temperature inhomogeneities at both ends of a linear heat source (end effect). So far, the differential arrangement of two heat sources was not realized with the THS.

Now, more than 25 years later, Gustafsson's method has evolved into the so-called transient hot-*bridge*(THB) technique [2]. This new measurement method, developed at Physikalisch-Technische Bundesanstalt (PTB), Germany, preserves all advantages of the strip but avoids its major drawbacks. THB uses a novel multiple strip on foil sensor. Eight strips are switched to a symmetrical Wheatstone bridge to provide effective thermal and electrical self-compensations.

The present paper highlights the theory and practice of the new THB method. It starts with the basic THS mathematical model and some of its later extensions valid for different intervals in time. Then, the three different modes of operation of the THB are analyzed and discussed. Finally, experimental results on two reference materials and thermal insulations are presented along with the preliminary estimated uncertainty in thermal conductivity.

2. TRANSIENT HOT-BRIDGE METHOD

The central part of the THB method is a novel thermoelectric sensor (cf. Fig. 1). It is realized as a printed circuit foil of nickel between two

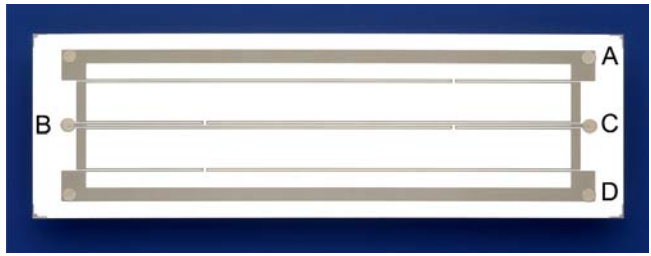

Fig. 1. Top view of the transient hot bridge sensor layout. Each of the four tandem-strips is 100 mm in length and 2 mm in width. Solder pads A, B, C, D: A-D, current source; B-C, DVM; (see Fig. 2) .

polyimide sheets. The sensor has an overall size of $109 \times 40 \times 0.06\,\text{mm}^3$ to fit between two sample halves of $100 \times 40 \times 20\,\text{mm}^3$ each. The layout of the sensor consists of four tandem strips in parallel. Each tandem strip comes in two individual strips, a short and a long one. Two of the tandems are located very close to each other at the center of the sensor and one additional tandem on either edge. All eight strips are symmetrically switched for an equal-resistance Wheatstone bridge (cf. Section 2.1). At uniform temperature, the bridge is initially balanced, i.e., no nulling is required prior to a run. An electric current makes the pairwise unequally spaced strips establish a predefined inhomogeneous temperature profile (cf. Section 2.2.) that turns the bridge into an unbalanced condition. From now on, the sensor produces an almost offset-free output signal of high sensitivity. This voltage rise in time is a measure of the thermal conductivity, λ, thermal diffusivity, a, and volumetric specific heat, $\rho\, c_\text{p}$, of the surrounding specimen. The signal is virtually free of thermal emf's because no external bridge resistors are needed. Each single strip is meander-shaped to give it a higher electrical resistivity. The segmentation into tandems compensates for the so-called end effect, i.e., the temperature drop at both ends of a linear or strip-shaped heater. In contrast to those bridges having some of their resistors located remotely from the measuring area, a THB sensor is completely surrounded by the specimen. Thus, no errors are introduced by the wiring of the bridge or any (external) noise pick-up.

2.1. Electrical Model

In the electrical model, all eight individual strips of the THB sensor, whether long or short, are treated as electrical resistors, R^{XY}. They are to be identified by their pair of superscripts, XY. The first superscript

indicates the location of the strip on the sensor, "I" stands for an inner (center) and "O" for an outer (edge) position. The second superscript informs about the strip's length, "L" and "S" denote long and short strips, respectively. For example, R^{IS} symbolizes a short inner strip.

Depending on the total length of the conducting path, long strips have a higher electrical resistance, R^{XL}, than short strips, R^{XS}. Together, all resistors act in an equal-resistance Wheatstone bridge as pictured in the equivalent circuit diagram, Fig. 2. Each of the four branches of the bridge consists of the same pair of a small and a high resistor; but, in opposing arms, their sequence is permuted. Due to this symmetry, there is no potential difference between points B and C as well as between points A and D. Since the bridge is initially balanced, no extra variable resistor for nulling is required. A current source is used for excitation. It may be applied across either set of opposite corners of the bridge.

For a given constant current input, I_B, applied between points A and D, the voltage drop, U_B, between points B and C, is given by

$$U_B = \frac{I_B}{2}\left[\left(\Delta R^{IL} - \Delta R^{IS}\right) - \left(\Delta R^{OL} - \Delta R^{OS}\right)\right] \tag{1}$$

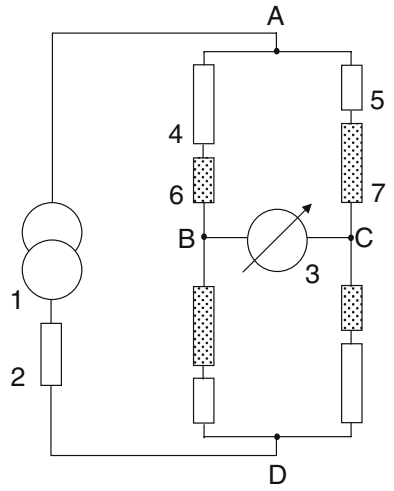

Fig. 2. Equivalent circuit diagram of the THB sensor (A-B-C-D) including current supply: 1, constant current source; 2, shunt; 3, DVM; 4, long outer resistor (R^{OL}); 5, short outer resistor (R^{OS}); 6, short inner resistor (R^{IS}); 7, long inner resistor (R^{IL}); (see text).

This result represents the output voltage of the THB sensor precisely because all resistors of the bridge change with temperature at the same amount. It should be noted that there is no linearity error. Regardless of its value, the stability of the excitation current, I_B, directly affects the overall accuracy of the bridge output, U_B (see Section 3.1).

During measurements, all eight resistors simultaneously act as resistance thermometers and Joule heaters. Each resistor generates heat at a rate,

$$\Phi = U_0 \frac{I_B}{2} = \frac{R_0^{XY} I_B^2}{4} \tag{2}$$

where U_0 is its voltage drop. As thermometers, the resistors are free to vary in time with their own temperature, $\Delta T^X(t)$. For a small temperature rise, the following linear expression is valid:

$$\Delta R^{XY}(T(t)) = R_0^{XY} \alpha \Delta T^X(t) \tag{3}$$

Here, α is the temperature coefficient of the initial electrical resistance R_0^{XY} at a reference temperature, $T_0 = T_0^I = T_0^O$. In the following, for convenience, this initial temperature is set to zero, $T_0 = 0$. Equation (3) links together the electrical and thermal models of the THB. The latter model will be discussed below.

Allowing for different temperature rises at the inner and outer strips, $\Delta T^I(t)$ and $\Delta T^O(t)$, respectively, and substituting Eq. (3) into Eq. (1) results in

$$U_B(t) = \frac{I_B}{2} \alpha \left[\Delta T^I(t) \left(R_0^{IL} - R_0^{IS} \right) - \Delta T^O(t) \left(R_0^{OL} - R_0^{OS} \right) \right] \tag{4}$$

Both differences in initial resistances are equal since the resistors are pairwise equivalent. Thus, the sensor output is given by

$$U_B(t) = \frac{I_B}{2} \alpha \left[\Delta T^I(t) - \Delta T^O(t) \right] \left(R_0^L - R_0^S \right) = \frac{\alpha I_B}{2} \Delta T(t) \Delta R_0 \tag{5}$$

So far, the bridge remains balanced even when heated homogeneously, $T^I(t) = T^O(t)$.

2.2. Thermal Model

The idea behind the THB technique is to create an inhomogeneous temperature profile inside the specimen by a characteristic *non-uniform* heating. For this purpose, the eight resistors of the sensor are arranged at positions from where they produce an axially symmetrical temperature

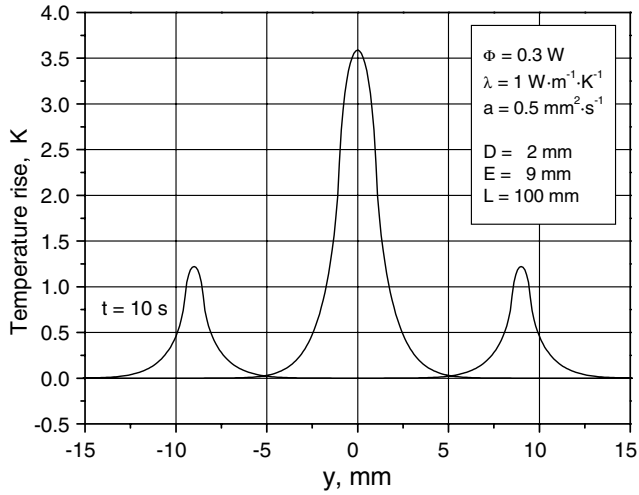

Fig. 3. Characteristic threefold temperature profile of a THB sensor across its width (y-axis) after a run time of 10 s as calculated in an ideal model (see text).

Table I. Parameter Set (BK7) for Analytical Calculations and Finite Element Simulations.

Parameter	Symbol	Value
Rate of heat flow	Φ	0.3 W
Thermal conductivity	λ	1.1 W· m^{-1}·K^{-1}
Thermal diffusivity	a	0.5 mm^2· s^{-1}
Strip width	D	2.0 mm
Distance bertween inner and outer strip	E	9.0 mm
Strip length	L	100.0 mm

profile of three characteristic maxima, a global one, $T^{\mathrm{I}}_{\max}(t)$, at the center of the sensor and two local maxima, $T^{\mathrm{O}}_{\max,i}(t)$, of identical height on either side (cf. Fig. 3 and Table I). Both differences in temperatures of the global maximum and each of the two local maxima drive the bridge off balance generating an output voltage change that is the measure of the thermal conductivity, thermal diffusivity, and volumetric specific heat of the specimen.

In order to derive working equations for the thermophysical properties mentioned, the characteristic threefold THB temperature profile has to be represented analytically. This three-dimensional transient Fourier field,

$T = T(x, y, z, t)$, is governed by the heat conduction equation which cannot be solved analytically for the sensor's complex layout. However, by progressively approximating this layout to a physical model that can be interpreted in terms of Gustafsson's fundamental theory of the hot strip [1], solutions for special cases of interest are found.

The following assumptions are made: each of the sensor's four tandem strips is considered as one continuous electrically conducting element of overall length L. That implies that there is no gap either between the two conducting paths of a single strip or between the two strips of a tandem (cf. Fig. 1). Both outer tandems of equal width $D = 2d$ liberate their heat individually whereas the two inner tandems behave as one gapless single hot strip of twice the typical width, $2D = 4d$. Thus, an outer hot strip liberates heat at a rate Φ/L per unit length, whereas the inner hot strip generates two times this rate, $2\Phi/L$. However, the rate of heat flow per unit area, $\Phi/(DL)$, is the same for all four hot strips (cf. Eq. (9)). The three strips themselves respond to their concerted heating with a rise of their individual temperatures that causes their electrical resistances, $\Delta R\left(T^{\mathrm{X}}\right)$, to increase as governed by Eq. (5). In summary, it is assumed that the four tandems of the sensor act like three compact metal strips according to Ref. 1.

In Ref. 1, an ideal hot strip of negligible thickness ($\Delta x \to 0$) and infinite length ($\Delta z \to \pm\infty$) is assumed. Thus, the Fourier field mentioned may be reduced from three to one spatial coordinate, $T = T(x \to 0, y, z \to \pm\infty, t)$. It is further assumed that the strip is embedded in an unbounded homogeneous specimen of isotropic thermal conductivity and thermal diffusivity. This condition lets the long axis of the sensor act as a virtual adiabatic boundary because of symmetrical temperature gradients on either sides. Across this boundary no heat is exchanged. Thus, the Fourier field may further be reduced to a half-plane, e.g., ($x = 0, y \geqslant 0$). In Ref. 1, the strip's rise in temperature is governed by

$$\Delta T(y, t) = T(y, t) - T(y, t{=}0) = \frac{\Phi}{4\sqrt{\pi} L\lambda} \int_0^{\sqrt{4at}} \operatorname{erf}\left(\frac{y+d}{\sigma}\right) - \operatorname{erf}\left(\frac{y-d}{\sigma}\right) \mathrm{d}\sigma. \tag{6}$$

Already at this stage, the known theory is slightly extended to handle different strips of any width ϑ and arbitrary locations, $y = y_0$:

$$T(y, t) = \frac{\Phi}{4\sqrt{\pi} L\lambda} \int_0^{\sqrt{4at}} \operatorname{erf}\left(\frac{(y-y_0)+\vartheta}{\sigma}\right) - \operatorname{erf}\left(\frac{(y-y_0)-\vartheta}{\sigma}\right) \mathrm{d}\sigma \quad T_0 = 0 \tag{7}$$

Carrying out the integration in Eq. (7) provides the basic relation for the temperature generated by 'any' hot strip and measured at some distance $y \neq 0$ from the central axis at time t.

$$T(y,t) = \frac{\Phi}{4\sqrt{\pi} L D \lambda} f(t) \tag{8}$$

where

$$\begin{aligned} f(t) = \sqrt{4at}\left[\operatorname{erf}\left(\frac{(y-y_0)+\vartheta}{\sqrt{4at}}\right) - \operatorname{erf}\left(\frac{(y-y_0)-\vartheta}{\sqrt{4at}}\right)\right] \\ -\frac{(y-y_0)+\vartheta}{\sqrt{\pi}} \operatorname{Ei}\left(\frac{-((y-y_0)+\vartheta)^2}{4at}\right) \\ +\frac{(y-y_0)-\vartheta}{\sqrt{\pi}} \operatorname{Ei}\left(\frac{-((y-y_0)-\vartheta)^2}{4at}\right) \end{aligned} \tag{9}$$

Adding the individual temperature profiles of the inner hot strip ($\vartheta = 2d$) at $y = 0$ and of one of the two outer strips ($\vartheta = d$) located at $y = \pm y_0$ gives

$$T(y,t) = T^{\mathrm{I}} + T^{\mathrm{O}} = T(y, y_0 = 0, t, \vartheta = 2d) + T(y, y_0, t, \vartheta = d) \tag{10}$$

A typical result of a half-plane temperature profile for five different times obtained from Eq. (9) is shown in Fig. 4. Adding up each pair of temperatures yields the plot presented in Fig. 5. Both mean temperature excursions of the inner and outer hot strips are obtained by integrating over the individual strip's widths;

$$\overline{T}^{\mathrm{I}}(y,t) = \frac{1}{2d} \int_0^{2\mathrm{d}} T(y, y_0 = 0, t, \vartheta = 2d) + T(y, y_0, t, \vartheta = d)\, \mathrm{d}y \tag{11}$$

and

$$\overline{T}^{\mathrm{O}}(y,t) = \frac{1}{2d} \int_{y_0-d}^{y_0+d} T(y, y_0 = 0, t, \vartheta = 2d) + T(y, y_0, t, \vartheta = d)\, \mathrm{d}y \tag{12}$$

The above integrations lead to two very complex relations from which no suitable working equation can be derived directly. However, the entire temperature excursion does not matter here but, merely, its short-term and long-term behaviors. These two special cases cover the vast majority of sensor applications. They come in three different modes of operation.

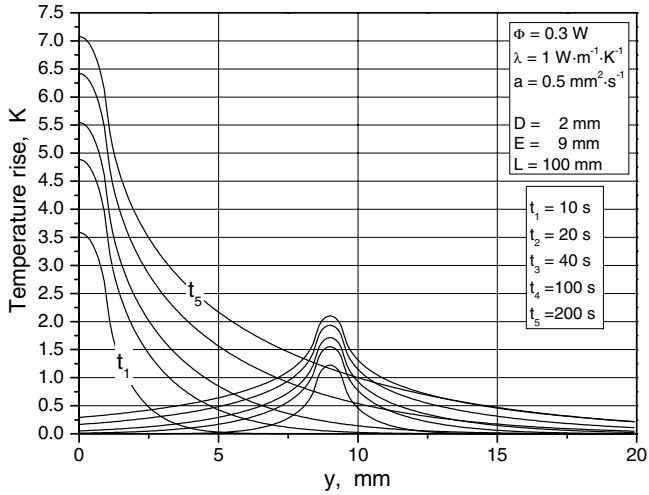

Fig. 4. Individual local temperature profiles of the inner and one of the outer hot strips for five different times calculated in an ideal model (see text).

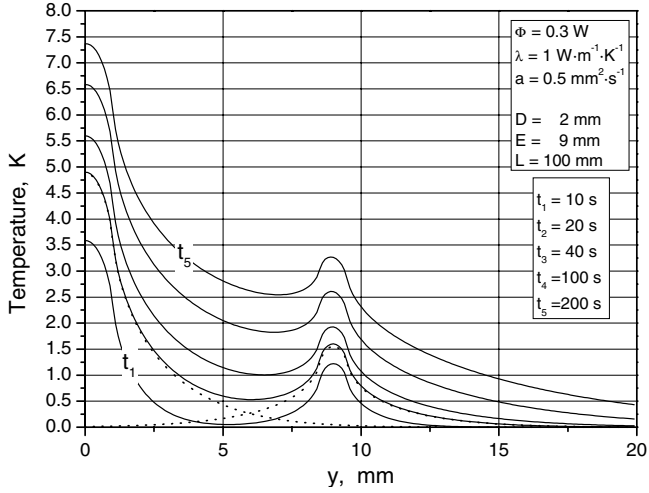

Fig. 5. Same local temperature profiles as in Fig. 4 but added up.

2.2.1. Basic Thermoelectric Mode of Operation

In the basic mode, the temperature profiles of the inner and outer hot strips are treated as independent (1) from each other and (2) from outer boundaries. These two restrictions allow use of the mathematical model of Eq. (6). By carrying out the first integration in time and subsequently a second one over the strip's width, the mean temperature in terms of the dimensionless time τ is obtained;

$$\overline{T}(\tau) = \frac{\Phi}{\sqrt{4\pi}\, L\lambda} f_0(\tau) \tag{13}$$

where

$$f_0(\tau) = \tau \operatorname{erf}\left(\tau^{-1}\right) - \frac{\tau^2}{\sqrt{4\pi}}\left(1 - \exp\left(-\tau^{-2}\right)\right) - \frac{1}{\sqrt{4\pi}} \operatorname{Ei}\left(-\tau^{-2}\right) \tag{14}$$

and

$$\tau = \frac{\sqrt{4at}}{D}. \tag{15}$$

The time τ is defined either by $\tau^{\mathrm{I}} = \sqrt{4at}/2D$ or by $\tau^{\mathrm{O}} = \sqrt{4at}/D$ for inner and outer strips, respectively. The mean temperatures of both these strips may now be evaluated separately. First, the difference in their temperatures is substituted into Eq. (5) keeping in mind that the inner hot strip generates twice the rate of heat flow as any outer strip.

$$U_{\mathrm{B}}(t) = \frac{\alpha\, \Delta R_0 I_{\mathrm{B}}}{2} \left\{ \frac{\Phi}{\sqrt{4\pi}\, L\lambda} \left[2 f_0\left(\tau^{\mathrm{I}}\right) - f_0\left(\tau^{\mathrm{O}}\right) \right] \right\} \tag{16}$$

This result is the fundamental relation of the basic mode of operation of the THB sensor. It represents the output signal best. However, Eq. (16) is nonlinear and implicit. Thus, the measurands cannot be derived analytically; rather they have to be estimated [1].

There are two first order approximations to Eq. (14), piecewise covering consecutive intervals in time. The first one [3] is valid for very short dimensionless times, $0 \leqslant \tau \leqslant 1$;

$$f_1(\tau) = \tau - \frac{\tau^2}{\sqrt{4\pi}} \tag{17}$$

and will surprisingly lead to a working equation of the volumetric specific heat (cf. Section 2.2.2). The second one, the quasi-linear relation, Eq. (18), closely approximates the complex function, Eq. (14), from $t_{\min} \approx D^2/a$ to

$t_{\max} \approx R^2/4a$ where R denotes the shortest distance from a hot strip to the outer surface (Refs. 4, 5, and 6).

$$f_2(\tau) = \frac{3-\gamma}{\sqrt{4\pi}} + \frac{2}{\sqrt{4\pi}} \ln\tau \tag{18}$$

Substituting Eq. (18) into Eq. (13) yields

$$\overline{T}(t) = \frac{\Phi}{4\pi L\lambda} \ln\left(\frac{45at}{D^2}\right). \tag{19}$$

This result directly represents the mean temperature excursion of an outer strip, $\overline{T}(t) = \overline{T}^{\mathrm{O}}(t)$. For an inner strip, the two substitutions $\Phi \to 2\Phi$ and $D \to 2D$ have to be applied:

$$\overline{T}^{\mathrm{I}}(t) = \frac{2\Phi}{4\pi L\lambda} \ln\left(\frac{45at}{4D^2}\right) \tag{20}$$

By subtracting both above relations, the governing equation of the basic thermal mode of a THB is obtained:

$$\overline{T}^{\mathrm{I}}(t) - \overline{T}^{\mathrm{O}}(t) = \Delta\overline{T}(t) = \frac{\Phi}{4\pi L\lambda} \ln\left[\frac{(45at)^2 D^2}{16D^4 45at}\right] = \frac{\Phi}{4\pi L\lambda} \ln\left(\frac{45at}{16D^2}\right) \tag{21}$$

$$\Delta\overline{T}(t) = \frac{\Phi}{4\pi L\lambda}\left[\ln(t) + \ln\left(\frac{45a}{16D^2}\right)\right] = m_{\mathrm{qlin}} \ln(t) + n_{\mathrm{qlin}} \tag{22}$$

Obviously, the output relevant temperature difference, $\Delta\overline{T}(t)$, remains quasi-linear in time. Compared with the outer hot-strip temperature rise, the THB-slope, $m_{\mathrm{qlin}} = \Phi/(4\pi L\lambda)$, is the same whereas the THB-intercept $n_{\mathrm{qlin}} = m_{\mathrm{qlin}} \ln\left(45a/16D^2\right)$ is smaller. The latter fact gives rise to a more precise evaluation of the thermal diffusivity of the material under test (see Eq. (25)).

Finally, the electrical and thermal models are combined according to Eq. (5). The output signal of the sensor will be

$$U_{\mathrm{B}}(t) = \frac{\alpha R_0^2 I_B^3}{8\pi L\lambda} \ln\left(\frac{45at}{16D^2}\right) \tag{23}$$

When plotted against $\ln t$, a straight line of slope m_{THB} and intercept n_{THB} is obtained for the voltage reading. From the slope, the thermal conductivity can be determined;

$$\lambda = \frac{\alpha R_0^2 I_B^3}{8\pi L m_{\mathrm{THB}}} \tag{24}$$

From the slope and intercept, the thermal diffusivity is calculated according to

$$a = 2.82 \exp\left(\frac{n_{\mathrm{THB}}}{m_{\mathrm{THB}}}\right) \tag{25}$$

For a given parameter set (see Table I) temperature excursions of the inner and outer hot strips are calculated analytically according to the above equations and plotted versus time in Fig. 6.

Operating the THB sensor in its basic thermoelectric mode (short-term approximation) implies that the cross section, $S = B^2$, of the sample under test ($B \approx 40\,\mathrm{mm}$) should comply with the typical width B of the sensor. The individual positions of the sensor's three hot-strips are chosen in accordance with the specimen's typical width to allow for both mutual (strip-to-strip) and environmental (strip-to-surroundings) interactions practically at the same time of measurement. In most cases, this special arrangement causes a clear transition from ideal to real conditions when outer boundaries become effective.

A significant practical advantage of the new sensor arises from the fact that changes in the ambient temperature, $\delta T\,(t)$, during a run are effectively compensated by the bridge circuit. If $\delta T\,(y = 0, t) = \delta T\,(y = +y_0,\ t) = \delta T\,(y = -y_0, t)$ is valid, there will be a total compensation of this

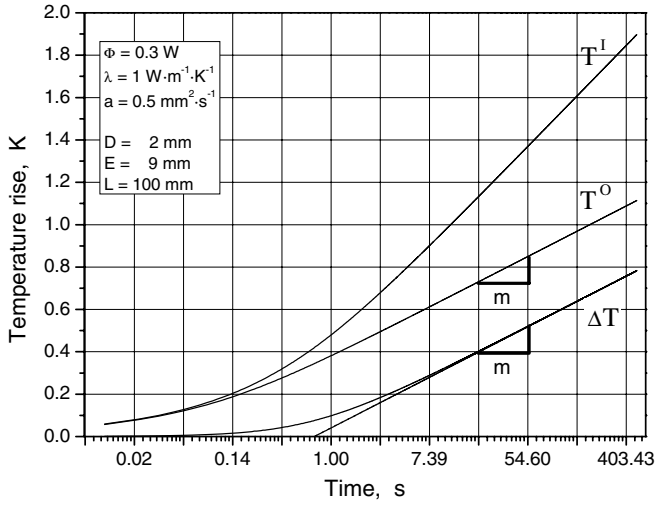

Fig. 6. Calculated temperature rises in time of the inner, T^I, and outer, T^O, hot strips and their differences in temperatures, ΔT: THB sensor output.

disturbance. As can be seen from the finite element simulation, Fig. 7, even the influence of adiabatic boundaries on the sensor output nearly vanishes ($\lambda, a = \text{const.}$). The remaining small difference in temperatures, Fig. 8, between isothermal and adiabatic boundaries originates from the different distances of the inner and outer strips to the outer boundary.

2.2.2. *Calorimeter Mode*

Recalling the short-term approximation, Eq. (17), and substituting it into Eq. (13) leads to the following relation for the difference in temperatures of the inner and outer hot strips:

$$\Delta\overline{T}(\tau) = \frac{\Phi}{\sqrt{4\pi}L\lambda}\left[\left(\tau^{\mathrm{I}} - \frac{(\tau^{\mathrm{I}})^2}{\sqrt{4\pi}}\right) - \left(\tau^{\mathrm{O}} - \frac{(\tau^{\mathrm{O}})^2}{\sqrt{4\pi}}\right)\right] \tag{26}$$

Recalculating in terms of real time t provides

$$\Delta\overline{T}(t) = \frac{2\Phi}{\sqrt{4\pi}L\lambda}\left(\frac{\sqrt{4at}}{2D} - \frac{4at}{\sqrt{4\pi}\,4D^2}\right) - \frac{\Phi}{\sqrt{4\pi}L\lambda}\left(\frac{\sqrt{4at}}{D} - \frac{4at}{\sqrt{4\pi}\,D^2}\right). \tag{27}$$

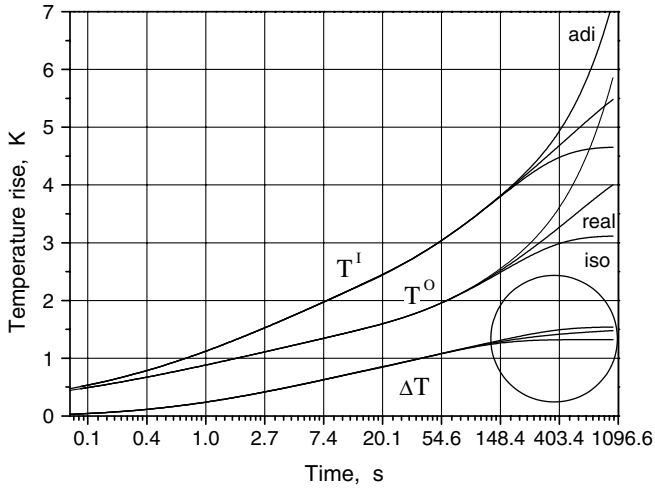

Fig. 7. FEM simulations of temperature rises in time of the inner, T^{I} and outer, T^{O}, hot strips and their differences in temperatures, Δ T: THB sensor output signals at different boundary conditions: adi, adiabatic; iso, isothermal; real, sample width 40 mm.

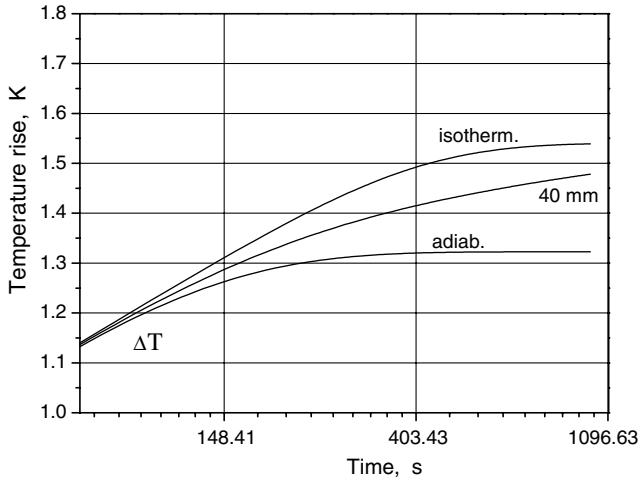

Fig. 8. Inset of Fig. 7: magnified presentation of long-term behavior of the sensor output signals for different boundary conditions.

Adding up all four terms and using the fundamental relation,

$$a = \frac{\lambda}{\rho\, c_{\mathrm{p}}} \tag{28}$$

finally results in

$$\Delta\overline{T}\,(t) = \frac{\Phi\, at}{2\pi\, D^2 L\lambda} = \frac{\Phi}{2\pi\, D^2 L\rho\, c_{\mathrm{p}}} t \tag{29}$$

Surprisingly, Eq. (29) represents a linear temperature rise depending on the volumetric specific heat $\rho\, c_{\mathrm{p}}$ of the specimen. Substituting Eq. (29) into Eq. (5) yields

$$U_{\mathrm{B}}\,(t) = \frac{\alpha\, R_0^2 I_B^3}{4\pi\, D^2 L\rho\, c_{\mathrm{p}}}\, t \tag{30}$$

When plotted against the real time t (cf. Fig. 9), the sensor voltage reading corresponds to a straight line of slope m_{lin}that (in the ideal model) passes through the origin (intercept: $n_{\mathrm{lin}} = 0$). Recalculating Eq. (30) furnishes the working equation for the volumetric specific heat,

$$\rho\, c_{\mathrm{p}} = \frac{\alpha\, R_0^2 I_B^3}{4\pi\, D^2 L\, m_{\mathrm{lin}}} \tag{31}$$

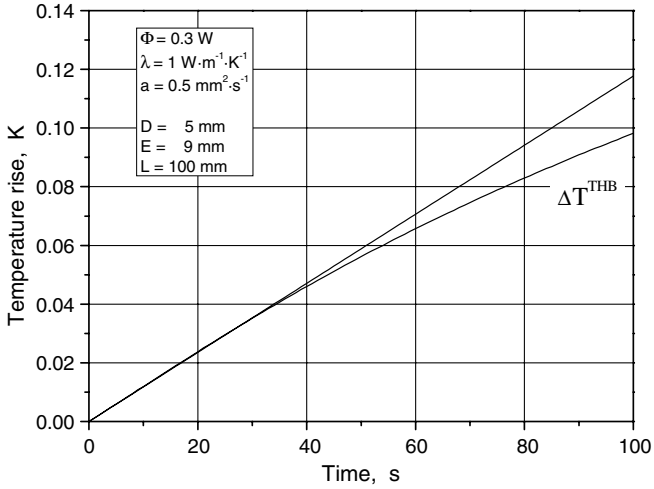

Fig. 9. Calculated short-term temperature excursion of the THB sensor output.

In practice, the intercept, n_{lin}, will not be equal to zero because of, e.g., the non-vanishing heat capacity of the sensor itself. The resultant delay can be taken as a measure of the time constant of the sensor.

The specific heat related volume, $V = \pi D^2 L$, is cylindrical with a radius $r = D$ and length L. Recalling Eq. (15) and recalculating this relation for the maximum time $t_{\max}$ of a specific heat experiment gives

$$t_{\max} \approx \frac{D^2}{4a} \tag{32}$$

For the THB sensor used so far, the time $t_{\max}$ will be too short for a precise measurement of the volumetric specific heat even for solids with a small thermal diffusivity $\left(a < 1\,\text{mm}^2 \cdot \text{s}^{-1}\right)$.

Therefore, when using the THB setup as a calorimeter, the sensor should have a strip width $D \geqslant 5\,\text{mm}$ (see Fig. 9) to establish a linear temperature rise of sufficient length. Groß et al. [7] used this linear short-time temperature excursion to measure the thermal conductivity in a regular hot-strip experiment on liquids.

2.2.3. Composite Thermoelectric Mode of Operation

So far, all individual temperature profiles inside the specimen were considered as absolutely independent from each other and from the outer boundaries, i.e., a sensor's hot strip senses neither the other strips nor the surroundings. In addition to this short-term case, the THB sensor offers

another attractive mode of operation by just using a larger specimen of width $B >> 40\,\text{mm}$ (cf. Fig. 10). In this long-term case, the strips can mutually interact for some time before the outer boundaries become effective. This allows for a quasi-steady-state measurement that starts directly after the transient output signal has passed over from the basic mode.

The working equation of this composite thermoelectric mode is derived the same way as above by adding up the two different temperature profiles of the sensor first;

$$T(y,t) = T^{\mathrm{I}} + T^{\mathrm{O}} = T(y, y_0 = 0, t, \vartheta = 2d) + T(y, y_0, t, \vartheta = d) \qquad (33)$$

and then calculating the two local mean temperatures, $\overline{T}^{\mathrm{I}}(t)$ and $\overline{T}^{\mathrm{O}}(t)$, in the half-plane $(x = 0, +y)$. It follows from symmetry reasons, $T^{\mathrm{I}}(y,t) = T^{\mathrm{I}}(-y,t)$, that $\overline{T}^{\mathrm{I}}(t)$ is identical to the mean temperature of the "right" half-strip of width D since

$$\begin{aligned} \overline{T}(t) &= \frac{1}{2d}\int_{-d}^{d} T(y,t)\,\mathrm{d}y = \frac{1}{4d}\int_{-2d}^{2d} T(y,t)\,\mathrm{d}y \\ &= \frac{1}{4d}\left[\int_{-2d}^{0} T(y,t)\,\mathrm{d}y + \int_{0}^{2d} T(y,t)\,\mathrm{d}y\right] \end{aligned} \qquad (34)$$

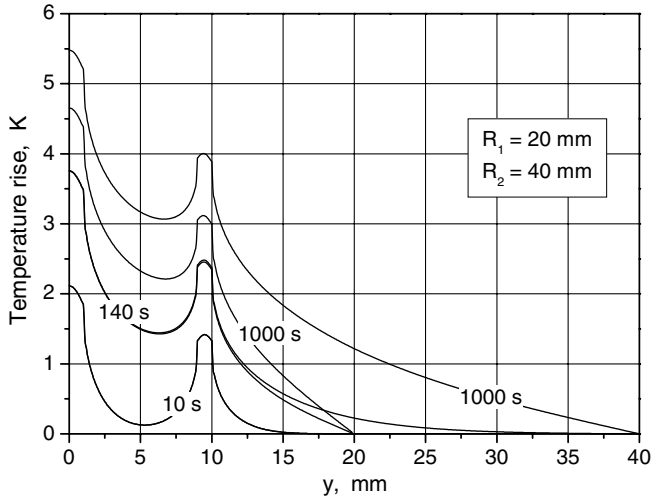

Fig. 10. Local temperature profiles for three different run times from FEM simulations for two different specimen sizes, R_1 and R_2, at isothermal boundary conditions.

Both mean temperature rises are obtained by

$$\overline{T}^{\mathrm{I}}(y,t)=\frac{1}{2d}\int_{0}^{2\mathrm{d}} T(y, y_0=0, t, \vartheta=2d)+T(y, y_0, t, \vartheta=d)\,\mathrm{d}y \tag{35}$$

and

$$\overline{T}^{\mathrm{O}}(y,t)=\frac{1}{2d}\int_{y_0-d}^{y_0+d} T(y, y_0=0, t, \vartheta=2d)+T(y, y_0, t, \vartheta=d)\,\mathrm{d}y \tag{36}$$

The above integrations, however, lead to two very complex relations from which no suitable working equation can be derived. Since, again, it's not the entire temperature excursion that matters here but the long-term behavior, it is sufficient to evaluate the limiting values of both of the above functions:

$$\lim_{t\to\infty} T^{\mathrm{I}}(y,t) = \frac{\Phi}{\pi L\lambda}\left[(y+2d)\ln\left(\frac{4at}{C(y+2d)^2}\right) - (y-2d)\ln\left(\frac{4at}{C(y-2d)^2}\right)\right] \tag{37}$$

$$\lim_{t\to\infty} T^{\mathrm{O}}(y,t) = \frac{\Phi}{2\pi L\lambda}\left\{\left[(y-y_0)+d\right]\ln\left(\frac{4at}{C\left[(y-y_0)+d\right]^2}\right) - \left[(y-y_0)-d\right]\ln\left(\frac{4at}{C\left[(y-y_0)-d\right]^2}\right)\right\} \tag{38}$$

In the above results, $C=\exp\gamma$ where γ denotes the Euler number. As has already been shown in principle in Ref. 3, both functions rapidly converge in time. By first adding up and then integrating Eqs (37) and (38), the mean values of the two individual temperatures are obtained. Subsequently subtracting one mean value from the other yields a dimensionless sensor constant, b, that is a function of d and y_0 only. Finally, the working equation for the secondary mode reads

$$\Delta\overline{T}^{\lim}=\frac{\Phi}{\pi L\lambda}b \tag{39}$$

3. EXPERIMENTS

On a first stage of testing the new method, finite element methods were performed to validate the design of the THB bridge sensor and to optimize its layout. Since "desk time is cheaper than test time", so-called virtual experiments were performed on the PC to vary most relevant parameters of the setup. Having obtained decisive answers on nearly all open design questions, prototypes of the sensor were built in-house and tested on the reference materials polymethyl methacrylate (PMMA) and BK7, a crown borosilicate glass. The results were surprisingly good. Now, a set of 40 sensors was fabricated using polyimide foils of 40 μm in thickness instead of the 25 μm thick foils of the home-made sensors. It turned out, that, especially, for good and very poor conducting materials, metals and thermal insulations, respectively, the uncertainty of the new sensor (typically 5%) was larger than expected. From an in-depth study on the influence of the base material of thermoelectric sensors on their uncertainty undertaken at the same time at PTB [11], it turned out that the polyimide foils have to be thinner to significantly reduce the uncertainty. Thus, the second lot of sensors is now based on polyimide foils of 25 μm each. The subsequently performed tests on thermal insulations, thus, were crucial (see below).

First, the new thin sensors were tested on the reference materials mentioned above. PMMA is an amorphous, colorless thermoplastic material of good abrasion resistance and dimensional stability. Its water absorptivity is very low in comparison with other polymers. In the past, PMMA has been successfully used at different institutes as a transfer standard for thermal conductivity [8]. The PMMA (Plexiglas®, Type GS) used here was produced by casting and supplied by Degussa Röhm Plexiglas GmbH. The thermal conductivity at 20°C is $\lambda = 0.1934\ \mathrm{W \cdot m^{-1} \cdot K^{-1}}$, and the thermal diffusivity at 20°C is $a = 0.120\ \mathrm{mm^2 \cdot s^{-1}}$ [7]. From THB measurements, the following results were obtained: $\lambda = 0.192\ \mathrm{W \cdot m^{-1} \cdot K^{-1}}$ and $a = 0.127\ \mathrm{mm^2 \cdot s^{-1}}$ which is for both results within the limits of the preliminary assessed uncertainty of the new method of 2% for thermal conductivity and 8% for thermal diffusivity. However, the thermal transport properties of PMMA are most similar to those of polyimide.

BK7 is a borosilicate glass that is widely used for optical systems and has been manufactured with outstanding homogeneity for several decades. The glass used here was manufactured and delivered by Schott AG. Previous investigations on this material indicate that the thermophysical properties are isotropic and have excellent long-term stability [9]. The THB measured thermal transport properties at 20°C are $\lambda = 1.11\ \mathrm{W \cdot m^{-1} \cdot K^{-1}}$ and $a = 0.57\ \mathrm{mm^2 \cdot s^{-1}}$ which again is in good agreement with the

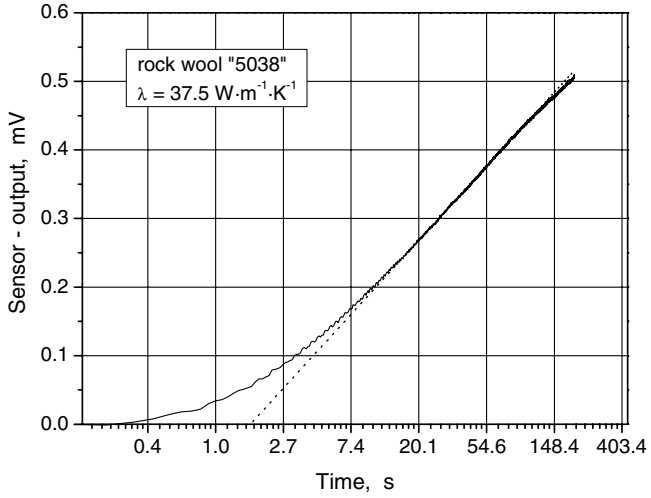

Fig. 11. Experimental sensor output signal for rock wool "5038" and linear approximation to determine the thermal conductivity.

preliminary reference data $\lambda = 1.09\,\mathrm{W \cdot m^{-1} \cdot K^{-1}}$ and $a = 0.538\,\mathrm{mm^2 \cdot s^{-1}}$ [9]. The uncertainty (see below) is 1.9%.

In close cooperation with Materialprüfanstalt Nordrhein-Westfalen (MPA NRW), Dortmund, Germany, a sample (rock wool "5041") of thick low density thermal insulation was measured. The MPA performed their measurements on a guarded hot-plate apparatus of $503 \times 503\,\mathrm{mm^2}$ metering area. It is the standard instrument for the certification of building materials of this facility with a carefully validated uncertainty of 1.5%. Their result at room-temperature is $\lambda = 38\,\mathrm{mW \cdot m^{-1} \cdot K^{-1}}$. MPA additionally used a THB sensor provided by PTB but driven and read out by a MPA homemade setup. Figure 11 shows the long-term sensor output signal of this rock wool fiber board. The result, $\lambda = 37.5\,\mathrm{mW \cdot m^{-1} \cdot K^{-1}}$, is in very good agreement (deviation: -1.3%) with the one mentioned above. Additionally, the short-term behavior of the output signal, Fig. 12, is evaluated. With the additional knowledge of the density of the fiber board ($\rho = 161\,\mathrm{kg \cdot m^{-3}}$) a specific heat $c_\mathrm{p} = 800\,\mathrm{kJ \cdot kg^{-1} \cdot K^{-1}}$ is calculated. So far, no reference values for this specimen are available.

Another thermal insulation material, Basotect, manufactured by BASFAG was tested at PTB. Basotect is a flexible open-cell foam material from melamine resin. It has high sound and heat absorption. Again, the thermal conductivity measured at room temperature, $\lambda = 29.2\,\mathrm{mW \cdot m^{-1} \cdot K^{-1}}$ (cf. Fig. 13), is in excellent agreement with that obtained from guarded

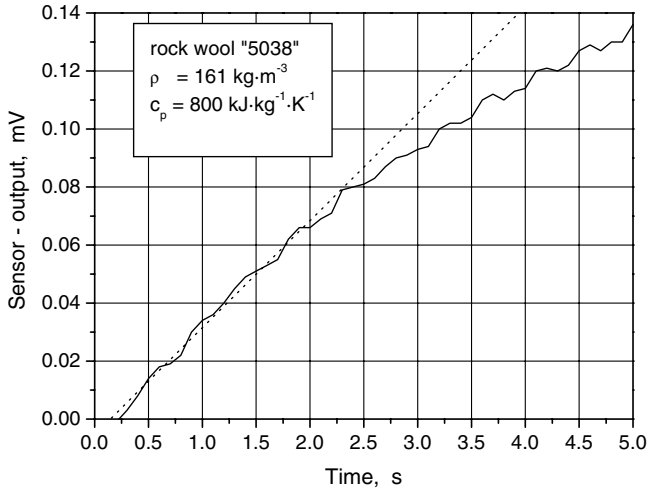

Fig. 12. Short-term experimental sensor output signal for rock wool "5038" and linear approximation to determine the volumetric specific heat.

hot-plate measurements, $\lambda = 29.7\,\mathrm{mW \cdot m^{-1} \cdot K^{-1}}$. The deviation between these two results of 1.7% is again within the limits of the uncertainty of the THB technique. While Basotect was measured using quasi-isothermal[4] boundaries made from thermostated quartz sand, a brick material with $\lambda = 0.51\,\mathrm{W \cdot m^{-1} \cdot K^{-1}}$ was analyzed at quasi-adiabatic boundaries made from wrapped light paper (cf. Fig. 14). The ends of both curves behave as expected from the finite element simulations. For a thermal insulation like Basotect, it is easy to experimentally maintain quasi-isothermal boundaries whereas quasi-adiabatic boundaries are very difficult to reach for very poor conducting materials. Therefore, a brick material of higher thermal conductivity was taken for the latter condition.

3.1. Measurement Uncertainty

Preliminary estimates of the uncertainty in thermal conductivity measurements using the new THB method have been carried out. The measurement on BK7 is taken as an example here. According to the ISO GUM [10], first, the standard uncertainties for each component according to the mathematical model, Eq. (24), were calculated. For convenience, all variables were treated as Type B. The systematic effect on any of them was assessed by its upper and lower bounds according to a rectangular

[4] The prefix "quasi" means as close as experimentally possible.

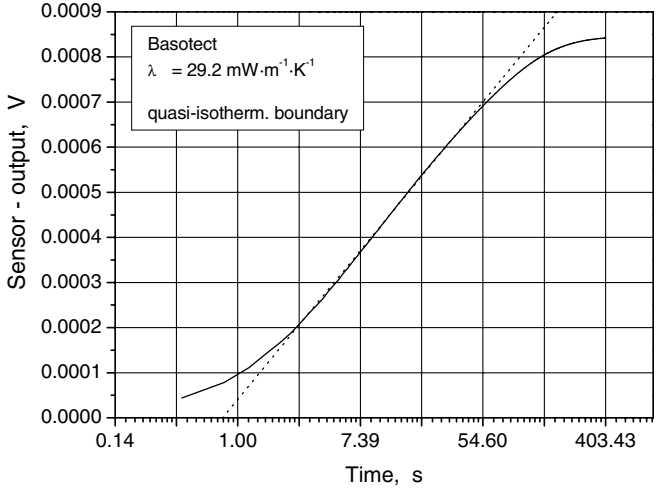

Fig. 13. Experimental sensor output signal for Basotect and linear approximation to determine the thermal conductivity at quasi-isothermal boundary conditions.

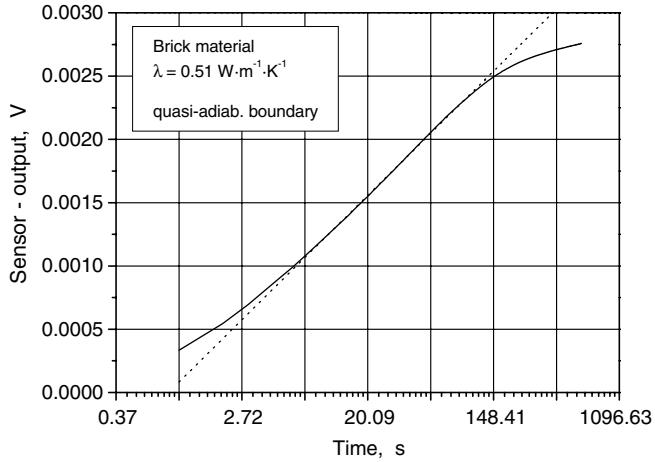

Fig. 14. Experimental sensor output signal for brick material and linear approximation to determine the thermal conductivity at quasi-adiabatic boundary conditions.

probability distribution (degree of freedom: ∞) (Table II). Secondly, the combined standard uncertainty was calculated. For the result in thermal conductivity, the expanded ($k = 2$) relative uncertainty of the measurement

Table II. Uncertainty Budget for a Thermal Conductivity Measurement on BK7.

Symbol	Value	Standard deviation	Sensitivity coefficient	Uncertainty u_x	Index
α	4.42×10^{-3}	0.784%	+ 250	8.7×10^{-3}	68.4%
R_0	3.26	0.100%	+ 0.68	2.2×10^{-3}	4.4%
I	0.5	0.069%	+ 6.7	2.3×10^{-6}	4.8%
L	0.1	0.289%	−11	-3.2×10^{-3}	9.3%
m	8.42×10^{-3}	0.343%	−130	-3.8×10^{-3}	13.1%
λ	1.110	0.948%			

on BK7 is ±1.9%. As can be seen from the "Index"-column of Table II, the major objective of possible improvements in the uncertainty of the sensor is a more precise determination of α, the temperature coefficient of the electrical resistance which, additionally, has the largest sensitivity coefficient. Next to this component, the length of the strip needs a more accurate determination.

As a result of the ideal model calculations and the finite element simulations performed so far, it was decided not to apply any correction to a result on a measurand of an influence quantity: the most important source for corrections involves deviations of the mathematical model from the experimental arrangement. Here, the ideal (mathematical) model of the THS technique is the basis for the working equations derived above. Calculations in this model were compared with finite element simulations on a FEM model that is very close to the practical version of the THB sensor (real model). Major discrepancies between the three models are listed in Table III. For the parameter set of Table I (BK7-data), the time development of local temperature profiles was calculated and simulated. Figure 15 shows six profiles along the y-axis for three different times. In the long-term behavior ($t = 1000$ s), the influence of the isothermal boundary at $R = 20$ mm is evident. However, until $t = 140$ s, at short-term conditions, the deviations between the ideal and the FEM models remain insignificant. The effect of the Kapton (foil) and the nickel (strip) can be perceived from Fig. 16 which is a magnified inset of Fig. 15. Due to its higher conductivity, the nickel ("FEM") causes a smaller curvature of the temperature profile across the strip width than does BK7 ("analyt."). The small difference in both curves at the center of curvature can be attributed to the (at this time constant) temperature drop across the insulation foil. At this early stage of uncertainty assessment, it can be concluded that the ideal model equations represent the basic thermoelectric model of the THB sufficiently precise. Next, the effect of the meandering of the strip will be analyzed analytically and in simulations. A complete assessment of the uncertainty is in progress.

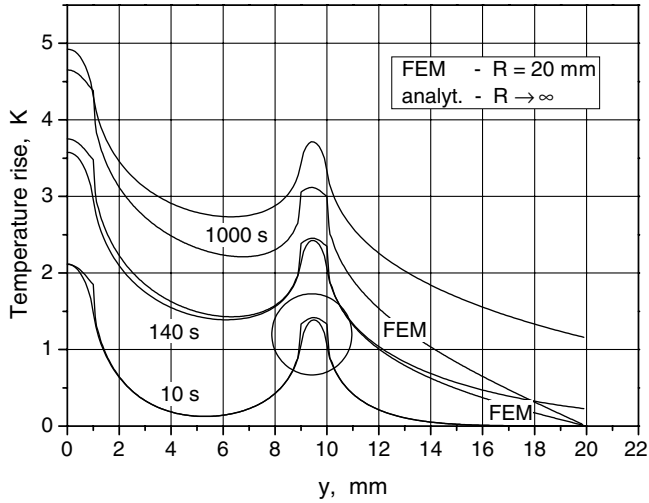

Fig. 15. Calculated and FEM-simulated local temperature profiles at three different times.

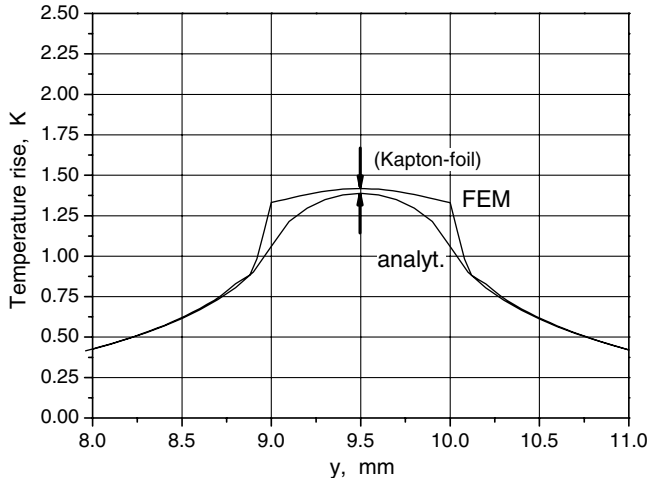

Fig. 16. Inset of Fig. 15: details of two different temperature profiles across the width of a hot strip.

Table III. Major Differences between the Ideal and Real Models.

	Ideal model	Real model	FEM model
Strip material	same as specimen	Nickel	Nickel
Strip shape	compact	Meandered	Compact
Strip surface	bare	Insulated	Insulated by Kapton
Specimen size	infinite	Bounded	Bounded

4. CONCLUSIONS

The latest descendant of the early nickel strip of the Gustafsson transient hot-strip technique is a "grown-up" thermal transport properties measuring device, the transient hot-bridge sensor. This advanced device avoids the major drawbacks of its predecessors but preserves nearly all of the advantages of the method. As the key component of a measuring instrument, the new thermoelectric sensor meets the specific needs of industry and research facilities for fast precise measurements at economical costs. From one single experiment on solids all three thermophysical parameters can be obtained after just a few minutes.

The idea behind the sensor is its equal-resistance Wheatstone bridge that, at uniform temperature, is initially balanced. During a test, a non-uniform temperature profile is generated that drives the bridge off balance and lets the bridge produce its offset-free output. There are three different modes of operation available yielding the thermal conductivity, thermal diffusivity, and the volumetric specific heat of the material under test from different intervals of the sensor output signal.

Measurements on the reference materials polymethyl methacrylate and the crown borosilicate glass BK7, on two thermal insulation materials, and a brick are presented. The preliminary assessed expanded standard uncertainty of the new method is about 2%.

For applications at temperatures above 220°C, the THB sensor was redesigned using ceramics as the base material instead of polyimide. At present, this so-called 'Janus' THB operates at temperatures up to 900°C [12].

ACKNOWLEDGMENTS

The authors would like to thank Dr. Regine Model of Physikalisch-Technische Bundesanstalt in Berlin for her valuable help by providing all FEM calculations of the so-called virtual experiment on the new sensor.

APPENDIX: HOT STRIP MEAN TEMPERATURE

Due to the non-uniform temperature profile across the width of a strip, the electrical resistance relevant temperature is the mean temperature $\overline{T}(y,t)$. Generally, this temperature is found by integration over a strip's width from $-d$ to d;

$$\overline{T}(t) = \frac{1}{2d} \int_{-d}^{d} T(y,t)\,\mathrm{d}y \tag{A1}$$

Instead of dealing with the above integral mean, the mean value theorem of integrals can be exploited as an uncomplicated way for determination of $\overline{T}$. According to the theorem mentioned, the mean temperature of a hot strip of half-width d can be found at a certain line $\overline{y} = nd$ parallel to the long axis ($y = 0$) at a distance $|\overline{y}|$. In the linear model of the basic THS theory [3], the coefficient n is obtained by equating the linear equation to the working equation of Gustafsson [1]. The transcendental equation results in

$$\frac{(n+1)^{n+1}}{|n-1|^{n-1}} = \frac{4}{\mathrm{e}} \Rightarrow\ n \approx 0.601 \tag{A2}$$

that can easily be solved numerically. The following simplified version of Eq. (A1) is also valid:

$$\overline{T}^{\,\mathrm{lin}}(t) = T(0.6d, t) \tag{A3}$$

This result can be very useful, especially for FEM simulations of hot strip arrangements, since no further integration has to be done over the strip's temperature profile.

REFERENCES

1. S. E. Gustafsson, E. Karawacki, and M. N. Khan, *J. Phys. D* **12**:1411 (1979).
2. U. Hammerschmidt, V. Meier, and R. Model, "New Transient Hot Bridge Sensor to Measure the Thermal Conductivity," in *Proc. 28*th *Int. Thermal Cond. Conf.,* St.Andrews-by-the-Sea, New Brunswick, Canada, 2005 (to be published).
3. S. E. Gustafsson, K. Ahmed, A. J. Hamdani, and A. Maqsood, *J. Appl. Phys.* **53**:6064 (1982).
4. U. Hammerschmidt, in *Proc. 24*th *Int. Thermal Cond. Conf.*, P. S. Gaal, ed. (Technomic, Lancaster, Pennsylvania,1999), pp. 123–134.
5. U. Hammerschmidt and W. Sabuga, *Int. J. Thermophys.* **21**:217 (2000).
6. U. Hammerschmidt, *Int. J. Thermophys.* **24**:1291 (2003).
7. U. Groß, Y. W. Song, and E. Hahne, *Fluid Phase Equilib.* **76**:273 (1992).

8. S. Rudtsch and U. Hammerschmidt, *Int. J. Thermophys.* **25**:1475 (2004).
9. S. Rudtsch, R. Stosch, and U. Hammerschmidt, in *Proc. 16*th *European Conference on Thermophysical Properties* (*ECTP 2002*), London (2002).
10. *Guide to the Expression of Uncertainty in Measurement* (ISO, Geneva, 1992).
11. R. Model, R. Stosch, and U. Hammerschmidt, "Improved Transient Hot Strip Sensor Design by Means of FEM Simulations," in *Proc. 28*th *Int. Thermal Cond. Conf.*, St. Andrews-by-the-Sea, New Brunswick, Canada, 2005 (to be published).
12. U. Hammerschmidt, V. Meier, and R. Model, "JANUS: High Temperature Transient Hot Bridge Sensor," in *Proc. 28*th *Int. Thermal Cond. Conf.*, St. Andrews-by-the-Sea, New Brunswick, Canada, 2005 (to be published).